JOURNAL OF COMPUTATIONAL PHYSICS 47, 109–129 (1982)

ADI on Staggered Mesh—A Method for the Calculation of Compressible Convection

KWING L. CHAN

Applied Research Corporation, 8401 Corporate Drive, Landover, Maryland 20785

AND

CHARLES L. WOLFF

NASA/Goddard Space Flight Center, Laboratory for Planetary Atmospheres, Greenbelt, Maryland 20771

Received September 8, 1981; revised December 11, 1981

An alternating direction implicit (ADI) method has been applied to a staggered grid for the computation of convection in a highly stratified fluid. Since artificial viscosity is not needed, subtle effects like the onset of convection can be studied. These computations compare well with the 2-*D* results by Graham and also agree with standard Boussinesq results when taken to that limit. Good efficiency has been achieved with a time step hundreds of times larger than the stability limit imposed by the explicit treatment of diffusion and the Courant number is not restricted to be below 1. The Navier–Stokes equation contains cross spatial derivatives which are treated explicitly in most ADI schemes. The destablizing effect of such a practice on a 2-*D* model system with second-order spatial derivative terms only was analyzed and found to be not excessive. When the fractional degree of implicitness β exceeds 0.572, it is sufficient to stabilize the model system. Our numerical experiments indicate that this is also a sufficient condition for the stability of the 2-*D* Navier–Stokes equation.

I. INTRODUCTION

Compressible convection is a common occurrence in nature. The numerical simulation or prediction of these kind of flows has wide application in fluid dynamics, meteorology, as well as astrophysics; however, it presents challenging difficulties. Because of the presence of gravity, the magnitude of the physical variables (e.g., density, pressure) often range over many orders of magnitude in the domain of interest. The velocity of the flow can be extremely subsonic in some important region. If the time step of a numerical scheme using an explicit method is restricted by the Courant condition on the sound travel time, the number of cycling steps required to advance the flow would be prohibitively large. On the other hand, if an implicit scheme is chosen to relax the time step restrictions, the coding becomes more complex and the amount of arithmetic per step increases substantially.

0021-9991/82/070109-21$02.00/0

To avoid the severe restriction imposed by the Courant condition, some people employ the Boussinesq approximation [1] or the anelastic approximation [2, 3], of the Navier–Stokes equations to avoid acoustical waves. The Boussinesq approximation is extremely unrealistic for highly compressible flows such as occur in deep atmospheres with many pressure or density scale heights (the e-fold vertical distances). The anelastic approximation is better; however, the assumption that the *deviations* of the variables from the *hydrostatic* values are small need not be true. At the upper region of an atmosphere, even small perturbations below can have devastating influence. Furthermore, the Mach numbers of compressible convection are usually not small (see Section III). Therefore, being able to handle the full Navier–Stokes equations for flows with a wide range of Mach numbers is a highly desirable feature for the numerical simulation of compressible convection.

In this paper, we describe a scheme which uses alternating direction implicit (ADI) method on a staggered mesh to treat this problem. Our motivation in developing such a scheme is to study large scale convection in the Sun. At the present stage, as a feasibility study, we have only tested this scheme in two spatial dimensions. It proves to be an efficient and accurate scheme for our purpose.

It is necessary to mention that the ICE method introduced by Harlow and Amsden [4] is able to handle compressible flow at a wide range of Mach numbers (see the applications in Cloutman *et al.* [5] and Cloutman [6]; also the extension to 3-D by Rivard and Torrey [7]). In this paper, however, we shall only discuss our experience with the ADI approach.

The ADI methods were first introduced by Peaceman and Rachford [8], and Douglas [9]. The original applications were the numerical calculation of the heat diffusion equation and the iterative solution of the discretized Laplace equation. Birkhoff *et al.* [10] have shown that this method is more effective than other iterative methods like the Seidel or SOR methods, particularly for refined meshes. Since that time, the alternating direction method has been continuously extended to include the treatment of general parabolic and hyperbolic problems (see Douglas and Gunn [11], and references therein). At the same time, several authors have studied some closely related techniques called methods of *fractional steps* [12].

The application of the ADI method to the calculation of multidimensional flow problems has flourished since the early seventies. Lindemuth and Killeen [13], and Briley and McDonald [14] independently devised closely related ADI schemes to solve nonlinear flow problems. They used a formal linearization (Taylor series expansion in time) for the nonlinear terms and reduced a multidimensional problem to the *noniterative* solution of a number of block tridiagonal matrices which can be handled efficiently [15]. Beam and Warming [16, 17] developed a similar scheme in *delta* form which has been widely applied in aerodynamical calculations [18, 19].

Even though the ADI method is popular in aeronautical calculations, its application to calculation of stratified flows is rare. Torrance [20] has used the ADI method to solve only the temperature equation in his computation of natural convection in a Boussinesq fluid.

With a staggered mesh system, the ADI scheme is stable without the need of

artificial viscosities [21]. This is a useful asset for studying problems in which the flow depends sensitively on the real viscosity (e.g., close to the onset of natural convection). Our program, which uses this scheme, has been successfully tested on computing convective rolls for a wide range of physical parameters. Steady state Mach numbers range from 10^{-2} to 0.3, depths of the layers up to 11 pressure scale heights, Courant numbers up to 10^2, and time steps in excess of the stability restriction imposed by explicit treatment of diffusion by a factor of 10^3.

In the next section, we shall describe our numerical methods in more detail. In Section III, we shall discuss some numerical experiments which test this scheme.

II. Numerical Method

A. *General Formulation*

Consider Cauchy problems of the following system of partial differential equations (PDE):

$$\frac{\partial}{\partial t} u_p = F_p \left(u_q, \frac{\partial u_q}{\partial x_\alpha}, \frac{\partial^2 u_q}{\partial x_\alpha \, \partial x_\beta} \right) \qquad 1 \leqslant p, \quad q \leqslant N, \tag{1}$$

where u_p are N dependent variables and x_α ($\alpha = 1,...$) are the spatial coordinates. An implicit finite difference approach is to approximate Eq. (1) by the following difference equations [22, 23]:

$$(u_p^{n+1} - u_p^n)/\Delta t = \beta F_p^{n+1} + (1-\beta) F_p^n + O(\Delta t) \qquad 0 \leqslant \beta \leqslant 1 \tag{2}$$

in which the superscript n is the time-step (cycle) number; $\beta = 0$ and 1 correspond to the forward (explicit) and backward (implicit) Euler time-differencing schemes, respectively.

For convenience, we shall use the notations:

$$D_\alpha u_q = \partial u_q / \partial x_\alpha = u_{q;\alpha}, \qquad D_{\alpha\beta} u_q = \partial^2 u_q / \partial x_\alpha \, \partial x_\beta, \qquad \Delta u_q^{n+1} = u_q^{n+1} - u_q^n,$$

$$\mathbf{F} = (F_1,..., F_N), \qquad \mathbf{u} = (u_1,..., u_N), \qquad x_\alpha x_\alpha = \sum_\alpha x_\alpha x_\alpha.$$

Also, define the operator $\mathscr{D}$ to be

$$\mathscr{D}_{pq} = (\partial F_p^n / \partial u_q) + (\partial F_p^n / \partial u_{q;\alpha}) D_\alpha + (\partial F_p^n / \partial u_{q;\alpha\beta}) D_{\alpha\beta}. \tag{3}$$

The value of F_p at the advanced time step $n+1$ can be obtained by the Taylor expansion

$$\mathbf{F}^{n+1} = \mathbf{F}^n + \mathscr{D} \, \Delta \mathbf{u}^{n+1} + O(\Delta u)^2. \tag{4}$$

Then difference equation (2) can be written as

$$(\mathbf{1} - \Delta t \beta \mathscr{D}) \, \Delta \mathbf{u}^{n+1} = \Delta t \mathbf{F}^n + O(\Delta t)^2, \tag{5}$$

where $\mathbf{1}$ is the identity matrix. The numerical algorithm of solving the Cauchy problem involves the following steps: (1) Calculate the value of $\mathbf{F}^n$ for the r.h.s. of Eq. (5) using known values of $\mathbf{u}^n$. (2) Solve linear equation (5) to obtain $\Delta\mathbf{u}^{n+1}$. (3) Update the value of $\mathbf{u}$ to the new time step by $\mathbf{u}^{n+1} = \mathbf{u}^n + \Delta\mathbf{u}^{n+1}$ and start a new cycle. Step 2 is a very laborious numerical process if the full linear system of equations are solved. The ADI method uses an approximate splitting technique to decompose the matrix $\mathbf{1} - \Delta t\beta\mathscr{D}$ into a product of matrices which are much easier to solve. The principle is to separate the spatial differential operators of different directions to form block tridiagonal matrices which can be solved *directly* by efficient algorithms. In our approach, we use a sparse matrix algorithm instead of the usual block elimination method [15]. The principles and the efficiencies of both methods are similar (see Section IIC).

The cross derivative terms $D_{\alpha\beta}u_q$ $(\alpha \neq \beta)$ pose a problem in the spatial splitting procedure. We follow the general practice of excluding them from the implicit treatment. This would not change the first-order accuracy of the temporal differencing. Moreover, the stability of the scheme is not seriously affected (see Section II.B).

Let $\mathscr{D}_0$ and $\mathscr{D}_\alpha$ $(\alpha = 1,...)$ be defined as

$$(\mathscr{D}_0)_{pq} = \partial F_p^n/\partial u_q, \qquad (\mathscr{D}_\alpha)_{pq} = (\partial F_p^n/\partial u_{q;\alpha})\, D_\alpha + (\partial F_p^n/\partial u_{q;\alpha\alpha})\, D_{\alpha\alpha}. \tag{6}$$

The ADI approximation of Eq. (5) can be written in the following form:

$$\prod_{\alpha=0,1,\ldots} (\mathbf{1} - \Delta t\beta\mathscr{D}_\alpha)\,\Delta\mathbf{u}^{n+1} = \Delta t\mathbf{F}^n + O(\Delta t)^2. \tag{7}$$

Notice that by carrying out the matrix multiplications on the l.h.s. and formally ignoring $(\Delta t)^2$ and higher order terms, one can obtain Eq. (5) (without the terms with cross derivatives). Sometimes, it is convenient (and natural) to absorb the terms of $\mathscr{D}_0$ into the $\mathscr{D}_\alpha$'s $(\alpha \neq 0)$ so that an extra matrix inversion can be avoided.

When the matrix equations of $(1 - \Delta t\beta\mathscr{D}_\alpha)$ are solved in successive steps, Eq. (7) represents a *consistent* discretization of Eq. (1). Alternative ways to choose the intermediate time steps between t^n and t^{n+1} can be employed [16, 22]. In those cases, however, one has to be careful whether the intermediate steps are consistent with the original equation. The lack of consistency would complicate the treatment of boundary conditions substantially (see [23] for a detailed discussion).

B. *Stability Analysis*

Suppose that $\tilde{\mathbf{u}}$ is the exact solution of Eq. (7), the propagation of numerical errors $\mathbf{e}$ can be derived by linearizing the r.h.s. of

$$\prod_\alpha (\mathbf{1} - \Delta t\beta\mathscr{D}_\alpha)(\tilde{\mathbf{u}}^{n+1} + \mathbf{e}^{n+1} - \tilde{\mathbf{u}}^n - \mathbf{e}^n) = \Delta t\mathbf{F}(\tilde{\mathbf{u}}^n + \mathbf{e}^n,...) \tag{8}$$

by means of Eq. (4). This gives

$$\mathbf{e}^{n+1} = \left[\prod_{\alpha} (1 - \Delta t\beta \mathscr{D}_\alpha)\right]^{-1} \left(1 + \Delta t \mathscr{D} - \Delta t\beta \sum_{\alpha} \mathscr{D}_\alpha\right) \mathbf{e}^n + O(e^2). \tag{9}$$

If the standard central differencing is used for the spatial difference operators, the error amplification matrix for the amplitude of a Fourier component $\exp(ik_\alpha x_\alpha)$ of $\mathbf{e}$ is given by

$$A = \left[\prod_{\alpha} (1 - \Delta t\beta \mathscr{D}'_\alpha)\right]^{-1} \left(1 + \Delta t \mathscr{D}' - \Delta t\beta \sum_{\alpha} \mathscr{D}'_\alpha\right), \tag{10}$$

where $\mathscr{D}'_\alpha$ and $\mathscr{D}'$ are matrices generating by replacing D_α, $D_{\alpha\alpha}$, and $D_{\alpha\beta}$ $(\alpha \neq \beta)$ in Eqs. (3) and (6) with $i \sin(k_\alpha \Delta x_\alpha)/\Delta x_\alpha$, $-4 \sin^2(k_\alpha \Delta x_\alpha/2)/(\Delta x_\alpha)^2$, and $-[\sin(k_\alpha \Delta x_\alpha)/\Delta x_\alpha][\sin(k_\beta \Delta x_\beta)/\Delta x_\beta]$, respectively. Since the value of k_α can only take the form $k_\alpha = \pi/l\,\Delta x_\alpha$, where $l \geqslant 1$, $\sin(k_\alpha \Delta x_\alpha)$ can be equal to zero but $\sin^2(k_\alpha \Delta x_\alpha/2)$ must be > 0. Therefore, in the above quantities, the one associated with $D_{\alpha\alpha}$ (at middle) is always negative, the others can be positive, negative, or zero. This is an important property associated with dissipative terms and their stabilizing effect on implicit numerical schemes.

For the scheme to be stable, the numerical errors must not grow. This requires that the absolute values of all eigenvalues of the amplification matrix be no greater than unity. Here we apply Eq. (10) to study the stability of some simple systems which illustrate important aspects of the compressible Navier–Stokes equations.

As a first example, let us consider the following system which represents the occurrence of linear waves with viscous damping

$$\frac{\partial u}{\partial t} = -c_1 \frac{\partial}{\partial x} v + d_1 \frac{\partial^2}{\partial x^2} u, \qquad \frac{\partial v}{\partial t} = -c_2 \frac{\partial}{\partial x} u + d_2 \frac{\partial^2}{\partial x^2} v, \tag{11}$$

in which $d_1, d_2 > 0$.

This one-dimensional system is relevant to problems with higher dimensions because the stability of individual components in an ADI scheme can ensure the stability of the whole scheme and vice versa [11].

Notice that if c_1 and c_2 are large, the matrix $\mathscr{D}$ is not diagonally dominated. For simplicity, let $e \equiv [\partial F_1/\partial u_{;xx}][4 \sin^2(k\,\Delta x/2)/\Delta x^2]$, $f \equiv [\partial F_2/\partial v_{;xx}][4 \sin^2(k\,\Delta x/2)/\Delta x^2]$, $g \equiv [\partial F_1/\partial v_{;x}][\sin(k\,\Delta x)/\Delta x]$, and $h \equiv [\partial F_2/\partial u_{;x}][\sin(k\,\Delta x)/\Delta x]$, then Eq. (10) can be written as

$$A = \begin{bmatrix} 1 + \Delta t\beta e & -i\,\Delta t\beta g \\ -i\,\Delta t\beta h & 1 + \Delta t\beta f \end{bmatrix}^{-1} \begin{bmatrix} 1 + \Delta t(\beta - 1)e & -i\,\Delta t(\beta - 1)g \\ -i\,\Delta t(\beta - 1)h & 1 + \Delta t(\beta - 1)f \end{bmatrix}. \tag{12}$$

The matrices in the numerator and denominator are simultaneously diagonalizable and the two eigenvalues of A are

$$\lambda_\pm = \frac{1 + \frac{1}{2}(\beta - 1)\,\Delta t\{e + f \pm [(e - f)^2 - 4gh]^{1/2}\}}{1 + \frac{1}{2}\beta\,\Delta t\{e + f \pm [(e - f)^2 - 4gh]^{1/2}\}}. \tag{13}$$

In order that $|\lambda_\pm| \leqslant 1$, β must satisfy the following inequalities:

$$\begin{aligned} &\beta \geqslant \tfrac{1}{2} - ((e+f)/2\Delta t(ef+gh)) && \text{for} \quad (e-f)^2 < 4gh \\ &\beta \geqslant \tfrac{1}{2} - (2/\Delta t\{e+f+[(e-f)^2-4gh]^{1/2}\}) && \text{for} \quad (e-f)^2 > 4gh. \end{aligned} \tag{14}$$

Since both e and f are positive, $\beta > \frac{1}{2}$ is sufficient to make the scheme unconditionally stable—this result is generally true when all terms in a differential equation are treated implicitly.

If the first-order spatial derivative terms (the wave terms) in Eq. (11) are not treated implicitly, the matrix $1 - \beta \Delta t \mathscr{D}$ is reduced to tridiagonal (instead of block tridiagonal). The scheme, however, will become unstable for *any* value of β when $\Delta t \gg \Delta x/(c_1 c_2)^{1/2}$.

The main goal of this section is to examine the destabilizing effect of excluding the cross derivative terms from the implicit treatment of the Navier–Stokes equations. The following simplified system can represent the specific situation very well:

$$\begin{aligned} \frac{\partial u}{\partial t} &= p\frac{\partial^2}{\partial x^2}u + q\frac{\partial^2}{\partial y^2}u + r\frac{\partial^2}{\partial x\,\partial y}v, \\ \frac{\partial v}{\partial t} &= p\frac{\partial^2}{\partial y^2}v + q\frac{\partial^2}{\partial x^2}v + r\frac{\partial^2}{\partial x\,\partial y}u, \end{aligned} \tag{15}$$

where $p, q > 0$. When u and v are interpreted to be velocities, the r.h.s. of Eq. (15) exactly yields the viscous terms of the Navier–Stokes equations in two dimensions when $p = \frac{4}{3}\nu_1 + \nu_2$, $q = \nu_1$, and $r = \frac{1}{3}\nu_1 + \nu_2$; ν_1 and ν_2 are the first and the bulk kinematic viscosities, respectively. We shall show that a sufficient condition for stability is

$$\beta > \tfrac{1}{2}[1 + (|r|/2(pq)^{1/2})] \geqslant \tfrac{1}{2}. \tag{16}$$

For the above system,

$$\mathscr{D} = \begin{bmatrix} pD_{11} + qD_{22} & rD_{12} \\ rD_{12} & pD_{22} + qD_{11} \end{bmatrix}. \tag{17}$$

Let

$$\begin{aligned} a &\equiv 4p \sin^2(k_x \Delta x/2)/\Delta x^2 + 4q \sin^2(k_y \Delta y/2)/\Delta y^2, \\ b &\equiv 4p \sin^2(k_y \Delta y/2)/\Delta y^2 + 4q \sin^2(k_x \Delta x/2)/\Delta x^2, \quad \text{and} \\ c &\equiv r[\sin(k_x \Delta x)/\Delta x][\sin(k_y \Delta y)/\Delta y], \end{aligned}$$

then

$$A = \begin{bmatrix} 1 + \Delta t\beta a & 0 \\ 0 & 1 + \Delta t\beta b \end{bmatrix}^{-1} \begin{bmatrix} 1 + (\beta - 1)\Delta t a & -\Delta t c \\ -\Delta t c & 1 + \Delta t(\beta - 1) b \end{bmatrix}. \tag{18}$$

Notice that the off-diagonal terms of the numerator do not contain β because they come from the explicit cross derivative terms. Since the denominator is a diagonal matrix, it can be inverted easily. To simplify manipulation, let us further define $d \equiv \Delta ta/(1+\Delta t\beta a) > 0$, $e \equiv \Delta tb/(1+\Delta t\beta b) > 0$, $f \equiv -\Delta tc/(1+\Delta t\beta a)$, and $g \equiv -\Delta tc/(1+\Delta t\beta b)$, then the eigenvalues of A can be expressed as

$$\lambda_{\pm} = \tfrac{1}{2}\{2-(d+e) \pm [(d-e)^2+4fg]^{1/2}\} \tag{19}$$

which are both real because $fg \geqslant 0$. The condition for stability is $|\lambda_{\pm}| \leqslant 1$ which is equivalent to $\lambda_+ \leqslant 1$ and $\lambda_- \geqslant -1$. These conditions are equivalent to: (i) $de \geqslant fg$, (ii) $4 \geqslant d+e$ and $(2-d)(2-e) \geqslant fg$. A sufficient condition for (i) and (ii) to be satisfied is that $d \geqslant |f|$, $e \geqslant |g|$, $2-d \geqslant |f|$, $2-e \geqslant |g|$, simultaneously. When Δt is large, the last two inequalities are more stringent than the first two and we can limit our attention to only the last two inequalities. For β, the last two inequalities become

$$\beta \geqslant \tfrac{1}{2}(1+|c|/a) - (1/\Delta ta) \qquad \text{and} \qquad \tfrac{1}{2}(1+|c|/b) - (1/\Delta tb).$$

Since $4\sin^2(k_x \Delta x/2)/\Delta x^2 > \sin^2(k_x \Delta x)/\Delta x^2$ for $k_x = \pi/l\,\Delta x$, $l \geqslant 1$ (same for y direction),

$$|c|/a \leqslant |r|/(pz+qz^{-1}) \qquad \text{and} \qquad |c|/b \leqslant |r|/(pz^{-1}+qz), \tag{20}$$

where $z \equiv |\sin(k_x \Delta x)/\Delta x|/|\sin(k_y \Delta y)/\Delta y|$. As functions of z, the maximum values of the r.h.s. of (20) are both $|r|/2(pq)^{1/2}$. Therefore, the sufficiency of condition (16) is proved. For the Navier–Stokes equations in two dimensions, if $\nu_2 = 0$, condition (16) becomes

$$\beta \geqslant 0.5(1+0.144) = 0.572. \tag{21}$$

Our numerical tests show that, most of the time, β can be chosen to be below this value and the program is still stable. The above inequality indeed only serves as a sufficient condition.

In actual computation, it is desirable to choose a value of β as close to 0.5 as possible. Sometimes, the convergence rate towards stationary solution can be enhanced this way.

C. *Manipulation of Matrices*

Not all of the matrices representing $\mathbf{1} - \Delta t\beta\mathscr{D}_\alpha$ are in block tridiagonal form originally. If the usual algorithm for solving block tridiagonal matrices is used, it is necessary to rearrange the arrays to put each of the matrices into block tridiagonal form. A more flexible way to solve these matrix equations is to use a sparse matrix technique (see [24, 25] and references therein). The matrices $\mathbf{1} - \Delta t\beta\mathscr{D}_\alpha$ are of the general form of Scheme 1 in which $X \cdots X$ represent blocks of nonzero matrix elements and the distances of the off-diagonal blocks to the diagonal are always equal. An important property of this kind of sparse matrix is that the LU decomposition of a nonsingular matrix has the form of Scheme 2 in which $L \cdots L$ and

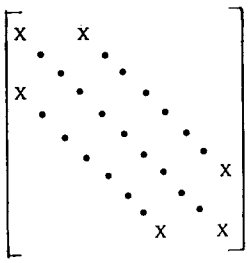

SCHEME 1

$U \cdots U$ are lower and upper triangular blocks. Gaussian elimination of this type of matrices is as efficient as the usual block elimination method. Even though the extra indexing required by a sparse matrix technique introduces overhead on operations, this disadvantage is counterbalanced by the automatic full exploitation of the sparseness of the system. Furthermore, such an approach can be generalized to other spatial differencing schemes (e.g., five-point differentation; upwind differencing) without any change on the matrix operation part of a program. Our subroutine for solving the sparse linear equations is based on the scheme discussed by Gustavson [24]. We tested the accuracy of the subroutine on ill-conditioned matrices as extreme as $|\lambda_{\min}| \sim 10^{-12} |\lambda_{\max}|$ with satisfactory results.

In our approach, the sparse matrices $1 - \Delta t \beta \mathscr{D}_\alpha$ and the indexing of their nonzero matrix elements are generated by a program called GENTRX [26]. Given two sets of discretized equations which represent the PDE in the two spatial directions, this program generates four subroutines in Fortran. Using symbolic differentiation, GENTRX creates two subroutines for computing the numerical values of the matrix elements at each time step. The other two provide indexing to keep track of the location of the nonzero elements. Before a calculation, the indexing routines are used (only once) to perform symbolic LU decomposition of the sparse matrices so that the process of solving the linear equations can be more efficient.

With the help of program GENTRX and the sparse matrix approach, the coding effort of adopting new boundary conditions or even new discretization schemes is reduced by a large factor. The demand of a program on core memory is

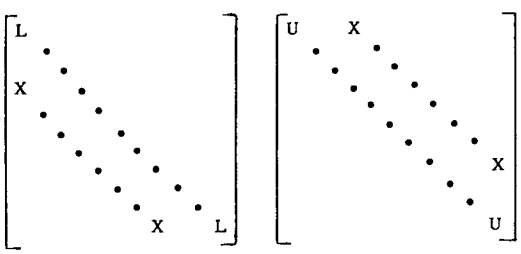

SCHEME 2

automatically reduced by the sparse matrix mode of storage. For example, a mesh with 22×27 grids in our program needs only 170 K byte for all the matrix elements (8 byte precision) and the indices.

D. *Discretization of the Navier–Stokes Equations*

We shall consider the Navier–Stokes equations in spherical coordinates (r, θ, ϕ) with axial symmetry; gravity is along the radial direction. By assuming $V_\phi = 0$, the system is reduced to two dimensional. With the existence of gravity and complications due to geometry, the 2-*D* equations cannot be written in a strong conservative form [27]. It is still useful, however, to keep the equations as conserving as possible [28]. This is especially valuable when the grid spacing in some region of the fluid (mostly at the top of a stratified fluid) is not small compared to the scale heights of the physical variables in the vertical direction. To obtain good spatial resolution, it is necessary to implement a nonuniform mesh system. In our program this was realized by a coordinate transformation

$$r = r(\xi) \tag{22}$$

in the r direction [29].

For convenience, let us define

$$\begin{aligned} &J = dr/d\xi, \qquad \Lambda = Jr^2 \sin\theta, \qquad D = \Lambda\rho, \qquad E = \Lambda\varepsilon, \\ &\mathbf{M} = \Lambda\rho\mathbf{V}, \qquad \boldsymbol{\tau} = \Lambda\boldsymbol{\sigma}, \qquad \mathbf{Q} = \Lambda\mathbf{q}, \\ &\Phi' = \Lambda\Phi, \qquad \mu' = \Lambda\mu, \qquad \zeta' = \Lambda\zeta, \qquad K' = \Lambda K, \end{aligned} \tag{23}$$

in which ρ is the density, ε is the internal energy per unit volume, $\mathbf{V}$ is the velocity, $\boldsymbol{\sigma}$ is the viscous stress tensor, $\mathbf{q}$ is the energy flux, Φ is the internal energy production rate due to viscous dissipation, μ, ζ are the first and the bulk viscosities, and K is the conductivity. Furthermore, the following notation is used:

$$\frac{\partial}{\partial s} = \frac{1}{r}\frac{\partial}{\partial\theta}, \tag{24}$$

and the subscripts r and s are used to denote the r and θ directions, respectively. Then the 2-*D* Navier–Stokes equations can be written as

$$\frac{\partial}{\partial t}D = -\frac{\partial}{\partial\xi}\left(\frac{M_r}{J}\right) - \frac{\partial}{\partial s}M_s, \tag{25}$$

$$\begin{aligned} \frac{\partial}{\partial t}E = &-\frac{\partial}{\partial\xi}\left(\frac{M_r E}{JD}\right) - p\frac{\partial}{\partial\xi}\left(r^2\sin\theta\frac{M_r}{D}\right) \\ &-\frac{\partial}{\partial s}\left(\frac{M_s E}{D}\right) - p\frac{\partial}{\partial s}\left(Jr^2\sin\theta\frac{M_s}{D}\right) - \frac{\partial}{\partial\xi}\left(\frac{Q_r}{J}\right) - \frac{\partial}{\partial s}Q_s + \Phi', \end{aligned} \tag{26}$$

$$\frac{\partial}{\partial t} M_s = -\frac{\partial}{\partial \xi}\left(\frac{M_r M_s}{JD}\right) - \frac{\partial}{\partial s}\left(\frac{M_s^2}{D}\right) - \frac{\partial p}{\partial \rho}\bigg|_\varepsilon \sin\theta \frac{\partial}{\partial s}\left(\frac{D}{\sin\theta}\right) - \frac{\partial p}{\partial e}\bigg|_\rho \sin\theta \frac{\partial}{\partial s}\left(\frac{E}{\sin\theta}\right) - \frac{M_r M_s}{rD} + \frac{\partial}{\partial \xi}\left(\frac{\tau_{sr}}{J}\right) + \frac{\partial}{\partial s}\tau_{ss} + \frac{1}{r}(\tau_{sr} - \cot\theta \tau_{\phi\phi}) \tag{27}$$

$$\frac{\partial}{\partial t} M_r = -\frac{\partial}{\partial \xi}\left(\frac{M_r^2}{JD}\right) - \frac{\partial}{\partial s}\left(\frac{M_s M_r}{D}\right) - Dg - \frac{\partial p}{\partial \rho}\bigg|_\varepsilon r^2 \frac{\partial}{\partial \xi}\left(\frac{D}{Jr^2}\right) - \frac{\partial p}{\partial \varepsilon}\bigg|_\rho r^2 \frac{\partial}{\partial \xi}\left(\frac{E}{Jr^2}\right) + \frac{M_s^2}{rD} + \frac{\partial}{\partial \xi}\left(\frac{\tau_{rr}}{J}\right) + \frac{\partial}{\partial s}\tau_{rs} - \frac{1}{r}(\tau_{ss} + \tau_{\phi\phi}), \tag{28}$$

where p is the pressure, g is the gravitational acceleration, and

$$\begin{aligned}
\tau_{rr} &= \frac{2\mu'}{J}\frac{\partial}{\partial \xi} V_r + \left(\zeta' - \frac{2}{3}\mu'\right)(\nabla \cdot \mathbf{V}) \\
\tau_{ss} &= 2\mu'\left(\frac{\partial}{\partial s} V_s + \frac{V_r}{r}\right) + \left(\zeta' - \frac{2}{3}\mu'\right)(\nabla \cdot \mathbf{V}), \\
\tau_{\phi\phi} &= 2\mu'\left(\frac{V_r}{r} + \cot\theta \frac{V_s}{r}\right) + \left(\zeta' - \frac{2}{3}\mu'\right)(\nabla \cdot \mathbf{V}), \\
\tau_{rs} &= \mu'\left[\frac{r}{J}\frac{\partial}{\partial \xi}\left(\frac{V_s}{r}\right) + \frac{\partial}{\partial s} V_r\right], \\
\nabla \cdot \mathbf{V} &= \frac{1}{J}\frac{\partial}{\partial \xi} V_r + \frac{\partial}{\partial s} V_s + \frac{2V_r}{r} + \frac{\cot\theta V_s}{r}, \\
Q_r &= -\frac{K'}{J}\frac{\partial}{\partial \xi} T, \qquad Q_s = -K'\frac{\partial}{\partial s} T, \\
\Phi' &= \mu'\left\{2\left[\left(\frac{1}{J}\frac{\partial}{\partial \xi} V_r\right)^2 + \left(\frac{\partial}{\partial s} V_s + \frac{V_r}{r}\right)^2 + \left(\frac{V_r}{r} + \frac{\cot\theta V_s}{r}\right)^2\right] \right. \\
&\quad \left. + \left[\frac{r}{J}\frac{\partial}{\partial \xi}\left(\frac{V_s}{r}\right) + \frac{\partial V_r}{\partial s}\right]^2\right\} + \left(\zeta' - \frac{2}{3}\mu'\right)(\nabla \cdot \mathbf{V})^2,
\end{aligned} \tag{29}$$

where T is the temperature. The implicit treatment of the above equations contains the following terms:

(i) in the s direction:

$$
\begin{aligned}
D&: -\frac{\partial}{\partial s} M_s, \\
E&: -\frac{\partial}{\partial s}\left(\frac{M_s E}{D}\right) - p\frac{\partial}{\partial s}\left(Jr^2 \sin\theta \frac{M_s}{D}\right) \\
&\quad + \frac{1}{r^2}\frac{\partial}{\partial s}\left\{K'\left[\frac{\partial T}{\partial \rho}\bigg|_\varepsilon \frac{\partial}{\partial s}\left(\frac{D}{J\sin\theta}\right) + \frac{\partial T}{\partial \varepsilon}\bigg|_\rho \frac{\partial}{\partial s}\left(\frac{E}{J\sin\theta}\right)\right]\right\}, \\
M_s&: -\frac{\partial}{\partial s}(V_s M_s) - \sin\theta\left[\frac{\partial p}{\partial \rho}\bigg|_\varepsilon \frac{\partial}{\partial s}\left(\frac{D}{\sin\theta}\right) + \frac{\partial p}{\partial \varepsilon}\bigg|_\rho \frac{\partial}{\partial s}\left(\frac{E}{\sin\theta}\right)\right] \\
&\quad + \frac{\partial}{\partial s}\left[2\mu' \frac{\partial}{\partial s}\left(\frac{M_s}{D}\right)\right], \\
M_r&: -\frac{\partial}{\partial s}(V_s M_r);
\end{aligned}
\tag{30}
$$

(ii) in the r direction:

$$
\begin{aligned}
E&: -\frac{\partial}{\partial \xi}\left(\frac{M_r E}{JD}\right) - p\frac{\partial}{\partial \xi}\left(r^2 \sin\theta \frac{M_r}{D}\right) \\
&\quad + \frac{1}{\sin\theta}\frac{\partial}{\partial \xi}\left\{\frac{K'}{J}\left[\frac{\partial T}{\partial \rho}\bigg|_\varepsilon \frac{\partial}{\partial \xi}\left(\frac{D}{Jr^2}\right) + \frac{\partial T}{\partial \varepsilon}\bigg|_\rho \frac{\partial}{\partial \xi}\left(\frac{E}{Jr^2}\right)\right]\right\}, \\
M_s&: -\frac{\partial}{\partial \xi}\left(\frac{V_r M_s}{J}\right), \\
M_r&: -\frac{\partial}{\partial \xi}\left(\frac{V_r M_r}{J}\right) - r^2\left[\frac{\partial p}{\partial \rho}\bigg|_\varepsilon \frac{\partial}{\partial \xi}\left(\frac{D}{Jr^2}\right) + \frac{\partial p}{\partial \varepsilon}\bigg|_\rho \frac{\partial}{\partial \xi}\left(\frac{E}{Jr^2}\right)\right] - Dg \\
&\quad + \frac{\partial}{\partial \xi}\left[\frac{2\mu'}{J^2}\frac{\partial}{\partial \xi}\left(\frac{M_r}{D}\right)\right].
\end{aligned}
\tag{31}
$$

Since our original purpose is to calculate convection in the Sun whose constituent is a nonideal gas which has very complicated thermodynamic behavior, we choose ρ and ε (instead of $\frac{1}{2}\rho V^2 + \varepsilon$) to be among the basic dependent variables in our equations. This choice simplifies the handling of the thermodynamics in the program substantially. Since the internal energy ε is not a conserved quantity, however, our energy equation is not in a conservative form. Therefore, truncation errors will affect the accuracy of total energy conservation of the system. In general, the thermodynamic functions (in terms of ρ and ε): p, T, $(\partial p/\partial \rho)_\varepsilon$, $(\partial p/\partial \varepsilon)_\rho$, $(\partial T/\partial \rho)_\varepsilon$,

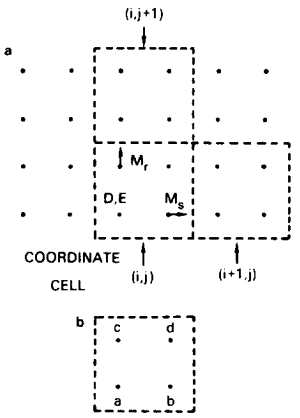

FIG. 1. Distribution of dependent variables on the staggered mesh.

$(\partial T/\partial \varepsilon)_\rho$, μ, ζ, and K are calculated at each time step by table interpolations. For an ideal gas, analytical formulas can be used:

$$p = (\gamma - 1)\,\varepsilon \tag{32}$$

$$T = (\gamma - 1)\,\varepsilon/\rho R, \tag{33}$$

where γ is the ratio of specific heats and R is the gas constant.

The discretization of all the above expressions is carried out in a staggered mesh system which is essential for avoiding the development of two grid interval waves without artificial viscosity [30]. Furthermore, as stressed by Messinger and Arakawa [30], it has the virtue of providing the same amount of accuracy with half the effort of using a nonstaggered mesh system. The distribution of dependent variables in the mesh is shown in Fig. 1. Each coordinate cell in the mesh is indexed by (i, j) in the (θ, ξ) directions and contains 4 locations (a, b, c, d) which are equally spaced in the θ-direction from neighboring locations. The vertical spacing can also be equal, or other configurations could be used to increase resolution at certain levels. The four basic variables D, E, M_s, and M_r are located at a, a, b, and c, respectively. Auxiliary variables are functions of these four and are defined at other locations by averaging whenever required. For example, the θ component of velocity at location c is written,

$$V_{sc}(i,j) = \frac{1}{2}\left[\frac{M_s(i,j)}{D(i,j)+D(i+1,j)} + \frac{M_s(i,j+1)}{D(i,j+1)+D(i+1,j+1)} + \frac{M_s(i-1,j)}{D(i,j)+D(i-1,j)} + \frac{M_s(i-1,j+1)}{D(i,j+1)+D(i-1,j+1)}\right] \tag{34}$$

and the discretization of the term $\partial(V_s M_r)/\partial s$ in the radial momentum equation takes the following form at the (i, j)th cell:

$$[V_{sc}(i+1,j)\,M_r(i+1,j) - V_{sc}(i-1,j)\,M_r(i-1,j)]/2\Delta s_c, \tag{35}$$

where $\Delta s_c = r_c(j)\,\Delta\theta$. At the beginning of each cycle, all the auxiliary variables are defined for the convenience of calculating the r.h.s. of Eqs. (25)–(28) and the matrix elements later.

III. Compressible Natural Convection in an Enclosed Container

Computation of compressible natural convection is a sensitive test on the accuracy and stability of a numerical method. In particular, the following points are noteworthy: (i) The onset of cellular convection depends very sensitively on the viscosity (or the Rayleigh number) and the boundary conditions. Introduction of artificial viscosity could shift the critical Rayleigh numbers to values much higher than the true ones. (ii) Conservation of mass in the enclosed container is very important, especially when the density near the top is very small compared to that near the bottom due to stratification. (iii) Physically, as well as numerically, a perturbation (or error) tends to grow much larger at the upper layers. Therefore, it is necessary to have an accurate approximation of the spatial dependence of the variables to avoid the development of catastrophic transients introduced by inexact initial conditions. An accurate spatial differencing is also important for the correct description of the subtle balance of viscosity and bouyancy which drives the convection. In our approach, central differencing provides good spatial accuracy and staggered mesh allows placing ρ and ε between the boundary and the nearest interior velocity grid points to improve stability at the boundary. Furthermore, mass is fully conserved in our discretization scheme.

In order that comparison can be made with previous results, we study the 2-*D* compressible convection of an ideal gas whose original distribution is polytropic. The linear stability of this problem has been studied by Spiegel [31] and Vickers [32]. A detailed numerical treatment of the nonlinear problem has been documented by Graham [33]. The numerical method employed by Graham was a modified two-step Lax–Wendroff scheme which suffers from both the Courant condition and the condition imposed by the explicit treatment of diffusion. As a result, most of his computations were limited to flows with Mach numbers $\gtrsim 0.1$ and low values of layer thickness (see IIIB).

A. *Definition of the Problem*

Consider an ideal gas confined in a box with $\theta_1 \leqslant \theta \leqslant \theta_2$, and $r_1 \leqslant r \leqslant r_2$. The boundary conditions are

$$V_r = \frac{\partial}{\partial r}\left(\frac{V_\theta}{r}\right) = 0, \qquad T = T_1, T_2 \qquad \text{at} \quad r = r_1, r_2 \tag{36}$$

and

$$V_\theta = \frac{\partial}{\partial \theta} V_r = \frac{\partial}{\partial \theta} T = 0 \qquad \text{at} \quad \theta = \theta_1, \theta_2. \tag{37}$$

We shall assume that the gas has constant specific heats (C_p, C_v), coefficients of viscosity (μ, ζ), and conductivity (K). The initial distribution of the gas is taken to be

$$T/T_2 = 1 + Z((r_2 - r)/(r_2 - r_1)), \tag{38}$$

$$\rho/\rho_2 = (T/T_2)^m, \tag{39}$$

$$p/p_2 = (T/T_2)^{m+1}, \tag{40}$$

where m, the polytropic index, and $Z \equiv (T_1 - T_2)/T_2$, the normalized thickness parameter, are constants. This represents a static solution of the Navier–Stokes equation with a uniform gravitational acceleration

$$g = (m + 1)\, ZRT_2/(r_2 - r_1). \tag{41}$$

To put the problem in dimensionless form, we scale the variables such that T_2, ρ_2, P_2, and r_2 at the upper boundary are all unity. In all our calculations we choose $(r_2 - r_1) = (\theta_2 - \theta_1) \leqslant 0.01$, and $\theta_2 = \pi/2$ so that the box approaches a square (aspect ratio = 1) and the results can be compared with those obtained by Graham. The value of m, the ratio of specific heats, and the Prandtl number $Pr \equiv C_p\mu/K$ will be fixed to be 1.4, 5/3, and 1, respectively. Therefore, the only free parameters left to specify the problem are Z, ζ/μ, and the Rayleigh number at the top

$$Ra = (PrgZ(r_2 - r_1)^3/(\mu^2/\rho_2^2))[(1 - (\gamma - 1)\, m)/\gamma]. \tag{42}$$

B. *Numerical Results*

Our first task was to study the ability of the present program to determine the critical Rayleigh number for the onset of convection in a 2-D square. As initial perturbation, a very small vertical velocity field was introduced to the fluid (with $\zeta = 0$), and its evolution was followed by the program (using a 22×42 uniform mesh) to determine whether the perturbation was growing or damping. After a few trials the critical Rayleigh number above which convection starts can be determined. Our results (small circles) are compared with those obtained by linear stability analysis computed by Graham (broken line) in Fig. 2. The agreement is better than 5% in all cases. The short solid line indicates the value of the critical Rayleigh number for a Boussinesq fluid [34]. At a small value of Z (0.1) we found the critical Rayleigh number very close ($\lesssim 2.5\%$ away) to this value [31].

Generally, the critical Rayleigh number we found is slightly higher than those obtained by linear stability theory. Tests show that a coarser mesh (22×27) causes the critical Rayleigh number to move a few percent farther from the ideal value. This indicates that the truncation errors in our spatial discretization tend to hinder the convective motion.

A comparison of maximum Mach numbers ($M_{\max}$) in stationary convective cells is shown in Fig. 3 for cases with $Z = 1$, $\zeta = 0$. The agreement is quite good even though our values are slightly lower than those of Graham. This again can be ascribed to the hindering effect of the spatial truncation errors.

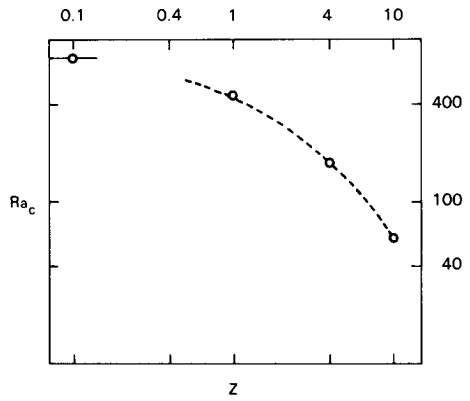

FIG. 2. Comparison of theoretical and computed values of critical Rayleigh numbers Ra_c at different thickness of stratification (Z): (---), critical Rayleigh numbers predicted by linear stability analysis; (O), results computed by the ADI program.

An interesting property of compressible convection can be observed in Fig. 3. A large range of Rayleigh numbers produces flow speeds which make compressible effects nonnegligible. Only a tiny range of Rayleigh numbers above the critical value produce really small Mach number flows. This phenomena persists for all other values of Z that we tested.

Since our program is able to handle unequal grid spacing in the vertical direction, we can obtain good resolution to study highly stratified cases (large Z). As an example, we describe here a case with $Z = 18$, $Ra = 50$, and $\zeta/\mu = \frac{2}{3}$; the ratio of pressure between the bottom and the top is greater than 10^3 (≈ 7 scale heights).

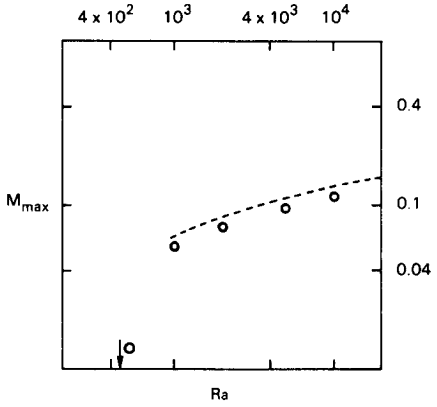

FIG. 3. Comparison of maximum Mach numbers at different Rayleigh number for $Z = 1$. (---), results inferred from Graham's paper; (O) results computed in the present study. The downward pointing arrow indicates the location of the critical Rayleigh number.

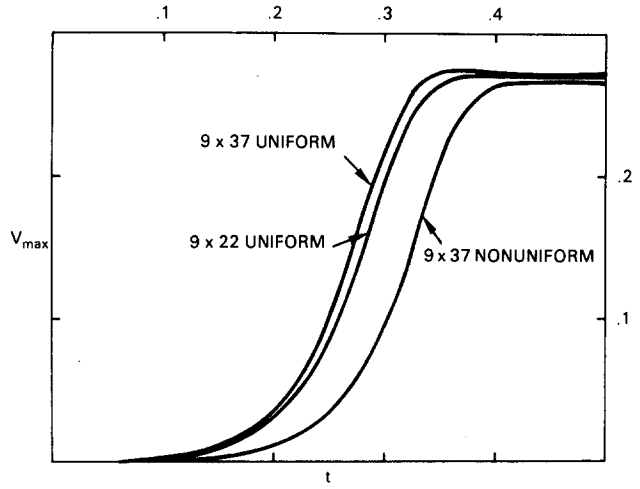

FIG. 4. Transients of the growth of V_{max} to stationary values for different mesh systems. The 9×37 nonuniform case has an initial velocity distribution slightly different from the others.

Three mesh distributions have been used for the computation: (i) a 9×37 mesh with unequal grid spacing, approximately 5 grid points per pressure scale height. (ii) a 9×37 uniform mesh. (iii) a 9×22 uniform mesh.

Let us define the following dimensionless numbers which specify how much the time step in our program violates the stability conditions of explicit methods:

$$N_{CFL} = \Delta t C_s / \Delta x \qquad \text{(Courant number)} \tag{43}$$

and

$$N_\nu = \Delta t \nu / \Delta x^2, \tag{44}$$

where C_s is the local sound speed, Δx is a local grid spacing, and ν is the kinematic viscosity. The transients of the calculations are illustrated in Fig. 4 by the maximum flow speed V_{max} which is given in units of $(p_2/\rho_2)^{1/2}$. The time steps used yield the following maximum values of (N_{CFL}, N_ν) respectively: (0.5, 108), (2.7, 17.2), (1.6, 5.9). Starting with a value of about 10^{-3}, the maximum flow speeds grow exponentially until asymptotic values are approached. The stationary values of all three cases agree to within 2.5% of each other. There are two reasons for the discrepancy of the asymptotic values of V_{max} between the uniform and nonuniform meshes. One reason is that the nonuniformity of a mesh introduces more truncation errors. Another reason is that, near the bottom of the box, the vertical grid spacing of the nonuniform mesh happens to be wider than those of the uniform meshes (more than 1.14 times). The stationary distribution of the velocity field of mesh (i) is shown in Fig. 5.

The above runs indicate that the uniform and coarser grids produce results quite

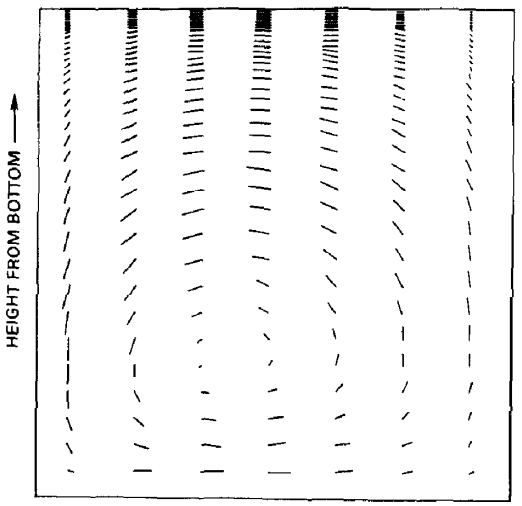

FIG. 5. The stationary velocity field of the 9×37 nonuniform case. The refined resolution clearly shows that the horizontal velocity decreases slightly near the top.

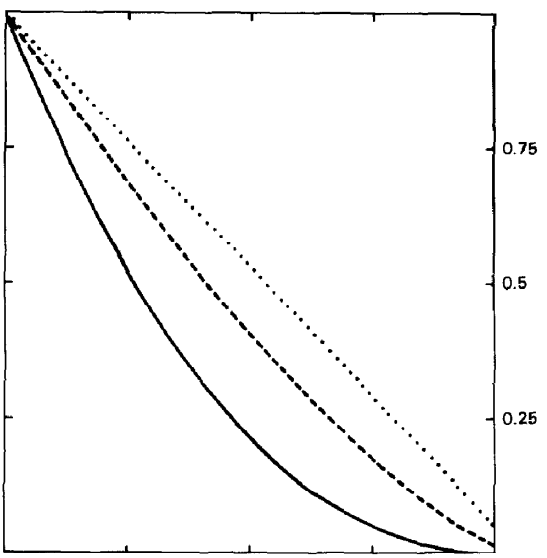

FIG. 6. Stationary distributions of the horizontal means of p (—), ρ (---), and T (···) versus height from the bottom. The uniform and nonuniform meshes produce almost identical results.

close to those with refined spatial resolution. To test this point further, we have computed cases with $Z = 100$, $\zeta/\mu = \frac{2}{3}$, and $Ra = 2$ using 9×37 and 9×22 uniform meshes; results are in agreement to within 6% of each other. In regimes where the stationary values of V_{max} fall below 0.01, however, agreement deteriorates quickly ($\gtrsim 25\%$) with the coarser grid generally yielding a lower value of stationary V_{max}.

It is useful to compare the 9×37 uniform and nonuniform spacing cases in more detail. The distributions of the horizontal means of ρ, p, and T are given in Fig. 6. The two cases give almost identical distributions. Comparison of values using interpolation shows that the relative differences are less than 1.5% everywhere; agreement improves tenfold near the bottom. This does not mean, however, that the finer spatial resolution can be discarded completely. When we plot the root-mean-square horizontal fluctuations of ρ, p, and T as shown in Fig. 7, the high resolution case shows spikes for ρ and p near the top of the fluid which were not clearly demonstrated by the equal spacing case. The existence of these spikes is related to the fact that the horizontal velocity decreases near the top as shown in Fig. 5. The pressure fluctuation is induced by the strong viscous stress of this shearing motion; the density follows the pressure fluctuation closely since the efficient conduction keeps the temperature fluctuation small at the top.

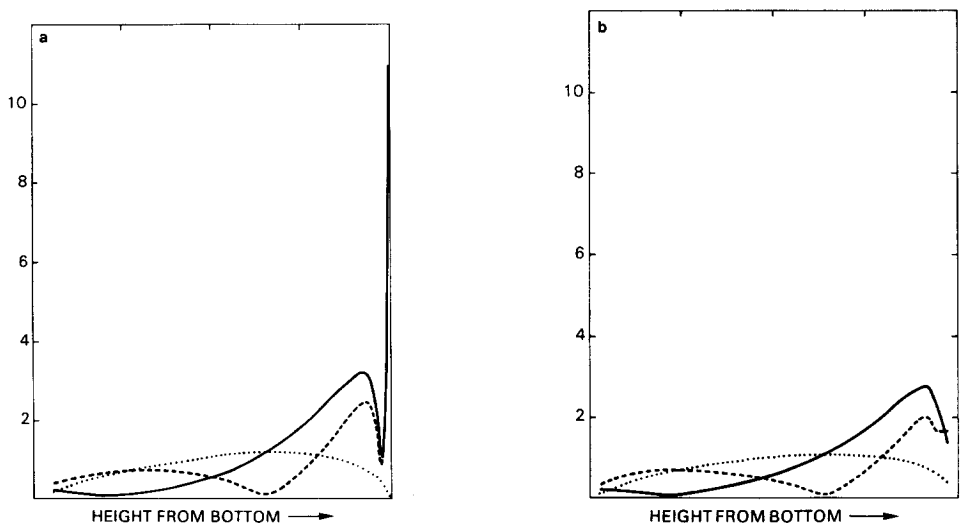

FIG. 7. Horizontal rms fluctuations of: p (—), ρ (---), and T (···) for (a) 9×37 nonuniform mesh (b) 9×37 uniform mesh. Vertical scale is in percentage.

IV. Summary and Discussion

In summary, the ADI and the staggered mesh work well with each other in providing an efficient and accurate implicit scheme for treating stratified flows. Due to the ability of taking large time steps, we can compute very subsonic flows for natural convection in a highly stratified medium without the introduction of Boussinesq or anelastic approximations whose assumptions were shown to be easily violated by compressible convections. The staggered mesh helps the accuracy of the scheme by avoiding the introduction of artificial viscosities; it also makes the handling of boundary conditions an easier job. The employment of the sparse matrix approach for solving the block tridiagonal matrices facilitates the adoption of new boundary conditions and even new discretization schemes.

Through the test cases, we verify that our approach is able to closely reproduce previous results obtained by other approaches (analytical as well as numerical computation using an explicit scheme).

Whether it is necessary to employ refined spatial resolution for highly stratified fluids depends on the objective of a computation. We have demonstrated that the gross features of convective flows are not seriously affected by a rough spatial resolution at the top. If a refined treatment can be skipped, a lot of computational effort can be saved. On the other hand, we have found that a good spatial resolution is very essential near the base of the fluid where most mass, energy, and momentum reside.

All the above computations were performed by a VAX 11/780 machine and the grind time (CPU per cycle per grid point) is about 7 msec (corresponding to $\sim$ 1.4 msec in IBM/360/91) which includes overhead due to page faults ($\approx$ 10–20%) caused by the limited usage of physical memories (150–350 K bytes). Eliminating the matrix generation and inversion in our program would make the scheme explicit, then the grind time is about $\frac{1}{3}$ of the above value. The implicit scheme, however, has allowed us to operate with time steps hundreds of times larger than in an explicit approach; thus it is much more economical. Our program carries a lot of burden for the intended application to nonideal gases which is unnecessary for computing perfect gases. Therefore, a reduction in the grind time can be obtained if the code is specialized and optimized further. Since our present interest is to sort out the fundamentals, however, this effort was not carried out in our study.

Compared to other implicit schemes, an advantage of the ADI approach is that it is noniterative. Therefore, the grind time is a constant independent of the number of grid points. This property is vital for computations which require big meshes.

An important problem concerning the ADI approach is the time accuracy of computing transients. When both N_{CFL} and $N_\nu \gg 1$, the ADI approach loses time accuracy completely, even though the steady state can eventually be recovered. On the other hand, we have some favorable experience with its time accuracy when N_{CFL} is moderately larger than 1 (below 10). However, our present understanding of this aspect is very incomplete; this question will be taken up in a later study.

ACKNOWLEDGMENTS

We would like to thank Drs. R. Warming, W. Briley, H. McDonald, and W. Sparks for helpful discussions in the beginning stages of this work, Dr. S. P. S. Anand for his encouragement and support, and we thank anonymous reviewers for their contributions toward improving the manuscript.

REFERENCES

1. J. BOUSSINESQ, "Theorie analytique de la chaleur," Tome II, Gauthier–Villars, Paris, 1903.
2. Y. OGURA AND J. G. CHARNEY, A numerical model of thermal convection in the atmosphere, *in* "Proceedings, Intern. Symp. Num. Wea. Prediction," Tokyo, 1962.
3. Y. OGURA AND N. A. PHILLIPS, *J. Atmospheric Sci.* **19** (1962), 173.
4. F. H. HARLOW, AND A. A. AMSDEN, *J. Comput. Phys.* **8** (1971), 197.
5. L. D. CLOUTMAN, C. W. HIRT, AND N. C. ROMERO, "SOLA-ICE: A Numerical Solution Algorithm for Transient Compressible Fluid Flows," Los Alamos Scientific Laboratory Report LA-6236, New Mexico, 1976.
6. L. D. CLOUTMAN, *Astrophys. J.* **227** (1979), 614.
7. W. C. RIVARD AND M. D. TORREY, Los Alamos National Laboratory Report LA-NUREG-6623, Supplement II, New Mexico, 1979.
8. D. W. PEACEMAN AND H. H. RACHFORD, *J. Soc. Ind. Appl. Math.* **3** (1955), 28.
9. J. DOUGLAS, *J. Soc. Ind. Appl. Math.* **3** (1955), 42.
10. G. BIRKHOFF, R. S. VARGA, AND D. YOUNG, Alternating direction implicit methods, *in* "Advance in Computers," Vol. 3, Academic Press, New York, 1962.
11. J. DOUGLAS AND J. E. GUNN, *Numer. Math.* **6** (1964), 428.
12. N. N. YANENKO, "The Method of Fractional Steps," Springer–Verlag, New York/Berlin, 1971.
13. I. LINDEMUTH AND J. KILLEEN, *J. Comput. Phys.* **13** (1973), 81.
14. W. R. BRILEY AND H. MCDONALD, Solution of the Three-dimensional compressible Navier–Stokes equations by an implicit technique, *in* "Proceedings, Fourth International Conference on Numerical Methods in Fluid Dynamics, Boulder, Colorado, June 1974," Springer–Verlag, New York/Berlin, 1975.
15. L. LAPIDUS AND J. H. SEINFELD, "Numerical Solution of Ordinary Differential Equations," Academic Press, New York, 1971.
16. R. M. BEAM AND R. F. WARMING, *J. Comput. Phys.* **22** (1976), 87.
17. R. F. WARMING AND R. M. BEAM, On the construction and application of implicit factored schemes for conservation laws, *in* "SIAM-AMS Proceedings," Vol. 11, 1977.
18. J. L. STEGER AND P. KUTLER, *AIAA J.* **15** (1976), 581.
19. T. H. PULLIAM AND J. L. STEGER, *AIAA J.* **18** (1980), 159.
20. K. E. TORRANCE, *J. Res. Nat. Bur. Stand. Sect. B* **72B** (1968), 281.
21. K. L. CHAN AND C. L. WOLFF, *Bull. Amer. Phys. Society* **25** (1980), 1102.
22. W. R. BRILEY AND H. MCDONALD, *J. Comput. Phys.* **24** (1977), 372.
23. W. R. BRILEY AND H. MCDONALD, *J. Comput. Phys.* **34** (1980), 54.
24. F. G. GUSTAVSON, Some basic techniques for solving sparse systems of linear equations, *in* "Sparse Matrices and Their Applications' (D. J. Rose and R. A. Willoughby, Eds.), Plenum, New York, 1972.
25. J. K. REID, Solution of Linear Systems of Equations: Direct methods (general), *in* "Sparse Matrix Techniques," Springer–Verlag, New York, 1977.
26. K. L. CHAN, "GENTRX: A Program for the Symbolic Generation of Sparse Matrices for the Implicit Treatment of PDEs," Applied Research Corp. Report No. TR-81-101, 1981.
27. M. VINOKUR, *J. Comput. Phys.* **14** (1974), 105.
28. K. BRYAN, *Mon. Weather Rev.* **94** (1966), 36.

29. F. G. BLOTTNER AND P. J. ROACHE, *J. Comput. Phys.* **8** (1971), 498.
30. F. MESSINGER AND A. ARAKAWA, "Numerical Methods Used in Atmospheric Models," GARP Publication Series No. 17, 1976.
31. E. A. SPIEGEL, *Astrophys. J.* **141** (1965), 1068.
32. G. T. VICKERS, *Astrophys. J.* **163** (1971), 363.
33. E. GRAHAM, *J. Fluid Mech.* **70** (1975), 689.
34. LORD RAYLEIGH, *Phil. Mag. Ser. VI* **32** (1916), 529.